50 kHz Capacitive Micromachined Ultrasonic Transducers for Generation of Highly Directional Sound with Parametric Arrays

Ira O. Wygant, *Student Member, IEEE*, Mario Kupnik, *Member, IEEE*, Jeffry C. Windsor, Wayne M. Wright, Mark S. Wochner, Goksen G. Yaralioglu, *Member, IEEE*, Mark F. Hamilton, and Butrus T. Khuri-Yakub, *Fellow, IEEE*

***Abstract*—In this study, we examine the use of capacitive micromachined ultrasonic transducers (CMUTs) with vacuum-sealed cavities for transmitting directional sound with parametric arrays. We used finite element modeling to design CMUTs with 40-μm- and 60-μm-thick membranes to have resonance frequencies of 46 kHz and 54 kHz, respectively. The wafer bonding approach used to fabricate the CMUTs provides good control over device properties and the capability to fabricate CMUTs with large diameter membranes and deep cavities. Each CMUT is 8 cm in diameter and consists of 284 circular membranes. Each membrane is 4 mm in diameter. Characterization of the fabricated CMUTs shows they have center frequencies of 46 kHz and 55 kHz and 3 dB bandwidths of 1.9 kHz and 5.3 kHz for the 40-μm- and 60-μm-thick membrane devices, respectively. With dc bias voltages of 380 V and 350 V and an ac excitation of 200 V peak-to-peak, the CMUTs generate average sound pressure levels, normalized to the device's surface, of 135 dB and 129 dB (re 20 μPa), respectively. When used to generate 5 kHz sound with a parametric array, we measured sound at 3 m with a 6 dB beamwidth of 8.7° and a sound pressure level of 58 dB. To understand how detector nonlinearity (e.g., the nonlinearity of the microphone used to make the sound level measurements) affects the measured sound pressure level, we made measurements with and without an acoustic low-pass filter placed in front of the microphone; the measured sound levels agree with numerical simulations of the pressure field. The results presented in this paper demonstrate that large-area CMUTs, which produce high-intensity ultrasound, can be fabricated for transmitting directional sound with parametric arrays.**

I. Introduction

For airborne ultrasound applications, capacitive transducers provide good transmit and receive sensitivity and a wideband frequency response. Other transducer technologies for generating airborne ultrasound include longitudinal-mode piezoelectric transducers, flextensional mode piezoelectric transducers, and PVDF (polyvinylidene fluoride) transducers. Conventional longitudinal-mode piezoelectric transducers—for example, longitudinal-mode transducers made from PZT (lead zirconate titanate)—are generally mechanically rugged and have good transmit sensitivity. However, their large mechanical impedance mismatch with air results in a narrowband frequency response; methods explored for increasing their bandwidth include impedance matching [1]–[3] and using piezoelectric composite materials [4]. Flextensional piezoelectric transducers [5]–[11] also provide large displacement amplitudes per applied volt and typically have narrow bandwidths; for large displacements, flextensional transducers can be highly nonlinear. Polyvinylidene fluoride (PVDF) transducers [12]–[14] in general have a low mechanical impedance and thus wide bandwidth and can be easily fabricated with different shapes and curvatures; however, a low dielectric constant, high dielectric loss, and low k_T limit their ability to produce high-intensity ultrasound [15].

Capacitive air transducers can be categorized into CUTs (capacitive ultrasonic transducers) and CMUTs (capacitive micromachined ultrasonic transducers). CUTs are manufactured by attaching a foil, commonly made of mylar or polyimide, to a grooved or pitted back plate (for example, see [16]). Conventional machining or microfabrication techniques create the grooves or pits. An insulating layer electrically isolates the foil from the back plate.

The volume of air in the pits or grooves strongly influences the CUTs' frequency response. Early methods used to fabricate CUTs could not precisely create cavities in the back plate. As a result, device performance was difficult to predict and control [17], [18]. Even with these limitations, capacitive transducers compare favorably with piezoelectric ultrasound transducers for operation in air [16]. The advent of micromachining, particularly silicon micromachining for microelectromechanical systems (MEMs), makes it possible to control the dimensions of the pits or grooves in the back plate precisely. This better control results in easier-to-design and better-performing devices [19]–[22].

CMUTs are capacitive transducers made entirely using microfabrication techniques [23], [24]. As a result, the CMUT membrane is a permanent part of the device and can be designed to tight geometric specifications. CMUTs can have air-filled cavities, like typical CUTs, or they can have have vacuum-sealed cavities. Because of the micro-

Manuscript received April 19, 2008; accepted July 18, 2008. This work was supported by DARPA SPAWAR Grant N66001-06-1-2032. Work was performed in part at the Stanford Nanofabrication Facility (a member of the National Nanotechnology Infrastructure Network), which is supported by the National Science Foundation under Grant ECS-9731293, its lab members, and the industrial members of the Stanford Center for Integrated Systems.

I. O. Wygant, M. Kupnik, G. Yaralioglu, and B. T. Khuri-Yakub are with the Edward L. Ginzton Laboratory, Stanford University, Stanford, CA (e-mail: iwygant@stanford.edu).

J. C. Windsor, W. M. Wright, M. S. Wochner, and M. F. Hamilton are with the Applied Research Laboratories, University of Texas at Austin, Austin, TX.

Digital Object Identifier 10.1109/TUFFC.2009.1019

machining methods used to seal the CMUT cavities, the cavity vacuum is expected to last indefinitely. Vacuum-sealed cavities avoid the damping effects of air inside the cavity and thus can improve transmit and receive sensitivity. However, for some low-frequency designs, vacuum-sealed cavities result in excessive static membrane displacement and stress; additionally, the damping effect of air inside the cavity is sometimes desired to increase the transducer's bandwidth.

There are two basic approaches to CMUT fabrication. First-generation CMUTs were made using sacrificial fabrication methods [25]. With these methods, built-up sacrificial material such as polysilicon defines the cavity volume. Material such as silicon nitride covers the sacrificial material. Removal of the sacrificial material leaves the membrane and cavity, which are the basic components of a CMUT. Recently, CMUT manufacturing methods based on wafer bonding [25] have gained popularity. Wafer-bonding methods provide tight control over device dimensions and result in a single-crystal silicon membrane, which has predictable mechanical properties. Additionally, wafer-bonded CMUTs are typically easier to fabricate. For the CMUTs designed for this study, wafer-bonding methods enable the large-diameter membranes and deep cavities that are required for low frequencies and high output pressures.

We designed the CMUTs in this study for transmitting highly directional sound. A directional sound source could be used, for example, in a quiet office space where the source transmits a narrow beam of sound that is audible only to listeners directly on-axis with the source. We generate the directional sound using the parametric array effect. The parametric array was first discovered by Westervelt in 1960 [26], [27] as a means of creating a beam of sound that is narrower than conventionally allowed by diffraction. Following its discovery, considerable work was done on parametric arrays in connection with its applications in underwater acoustics; however, there has been much less attention devoted to the parametric array in air. The first report of an experiment with a parametric array in air was published in 1975 by Bennett and Blackstock [28]. Subsequent work focused in large part on signal processing issues connected with the generation of audio sound having minimal distortion (see, e.g., Yoneyama *et al.* [29], Kite *et al.* [30], Pompei [31], [32], and Kim and Sparrow [33]) rather than on transducer design.

To generate directional low-frequency sound with a parametric array, the transducer transmits an amplitude-modulated ultrasound carrier wave. As this wave propagates, it becomes increasingly distorted due to the nonlinearities of sound propagation [34]. These nonlinearities result in the generation of harmonic components in the audio frequency band (in addition to higher harmonics), a process often referred to as self-demodulation. The beamwidth of the self-demodulated sound is similar to that of the carrier wave, yet at a much lower frequency. In other words, the beamwidth of the demodulated sound is much narrower than it would be had the sound been radiated directly by the transducer. For example, consider a transducer that transmits an amplitude-modulated ultrasound signal with carrier frequency f_0 and modulation frequency $f_{\text{diff}}/2$. The modulated signal consists of ultrasonic frequencies $f_1 = f_0 - f_{\text{diff}}/2$ and $f_2 = f_0 + f_{\text{diff}}/2$, which are referred to as the primary frequencies. As this signal propagates, self-demodulation results in audible sound at the difference frequency $f_{\text{diff}} = |f_2 - f_1|$. The challenge of transmitting sound with parametric arrays in air is to generate ultrasound waves with sufficient intensity to produce desirable sound pressure levels in the audio band.

In this paper, we examine the use of CMUTs for generation of high-intensity ultrasound for parametric arrays. We present the finite element model (FEM) simulations used to make two CMUT designs. We describe a fabrication process for making CMUTs with large diameter membranes and deep cavities. Finally, we discuss the characterization of the fabricated CMUTs and present measurements and simulations of the transmission of highly directional 5 kHz sound.

II. Design

We designed the CMUTs for an ultrasound carrier frequency of 50 kHz and a dc bias voltage of less than 1000 V. We chose a 50 kHz carrier frequency as a tradeoff between being sufficiently high to produce a reasonably narrow sound beam and being sufficiently low to avoid excessive absorption due to viscosity, heat conduction, and molecular relaxation in the air [35]. Limiting the bias voltage to less than 1000 V allows us to use an insulating layer thickness of several micrometers, which is a thickness easily grown with thermal oxidation and which is comparable to the insulating layer thicknesses successfully used in previously demonstrated CMUT designs.

The key device dimensions for the design of a single CMUT cell, as illustrated in Fig. 1, are the membrane thickness, membrane diameter, and cavity depth. We designed these dimensions using an axisymmetric finite element model (FEM) of the CMUT (implemented with Ansys Multiphysics Version 11 SP1, ANSYS Inc., Canonsburg, PA). This FEM accounts for the nonlinear effects (using the ANSYS nlgeom command) that result when the membrane deflects a large amount relative to its thickness [36]. We first used the FEM to predict membrane diameters and membrane thicknesses that would result in resonance frequencies close to 50 kHz. For design of the cavity depth, we used the model to estimate collapse voltage (in MEMS literature, the collapse voltage is commonly referred to as the pull-in voltage [37]); the collapse voltage is the maximum value of the dc bias voltage for a conventionally operated CMUT.

A prestressed modal analysis [38] of the FEM was used to predict resonance frequency as a function of membrane diameter and thickness (Fig. 2). For this analysis, a static analysis first calculated the membrane's stress due to atmospheric pressure. The mode frequencies and mode

TABLE I. DESIGN DIMENSIONS.

Design	A	B
Membrane diameter (mm)	4	4
Membrane thickness (μm)	40	60
Cavity depth (μm)	36	16
Oxide thickness (μm)	3.3	3.3

TABLE II. DESIGN CALCULATIONS AND SIMULATION RESULTS.

Design	A	B
Resonance Frequency, FEM (kHz)	46	54
Membrane Center Deflection from Atmospheric Pressure, FEM (μm)	27	9.9
Collapse Voltage, FEM (V)	880	620
Center Deflection with 80% of Collapse Voltage Applied, FEM (μm)	29.0	11.3
Ratio of Center Deflection to Average Deflection (r_{pk2avg}), FEM	3.2	3.2
Maximum Average Displacement from (1) (μm)	1.92	1.32
Maximum RMS Pressure Predicted from (2) (dB re 20 μPa)	138	136

shapes were then calculated based on the stressed model. Note that as the membrane becomes increasingly thin, its static deflection due to atmospheric pressure increases. As a result, the nonlinear effects of large membrane displacements [36] increasingly influence the resonance frequency. In Fig. 2, these effects explain why the 40-μm- and 50-μm-thick membranes have similar or higher resonance frequencies than thicker membranes. Ignoring the nonlinearity arising from large deflections can result in significantly different membrane resonance frequencies and static deflections. For example, ignoring these nonlinearites for the 40-μm- and 50-μm-thick membranes with 2 mm radii results in resonance frequencies of 38.0 kHz and 47.5 kHz rather than 45.5 kHz and 47.6 kHz. Furthermore, the predicted static deflections are 31.0 μm and 15.9 μm rather than 27.0 μm and 16.0 μm. Properly considering thin membranes is particularly important because thinner membranes provide wider bandwidths.

Based on the resonance frequency FEM analysis, we chose two membrane designs for fabrication (Table I). These designs have membrane diameters of 4 mm and membrane thicknesses of 40 μm and 60 μm. We chose cavity depths for these designs with predicted collapse voltages of 888 V and 620 V (Table II) to span a range of bias voltages less than 1000 V.

Because the CMUTs' cavities are sealed under vacuum, atmospheric pressure in addition to a dc bias voltage results in static membrane deflection (Fig. 3). For the 2 device designs, we used the FEM to calculate the static deflection at the membrane's center with a dc bias voltage equal to 80% of the collapse voltage (Table II). From this calculated deflection, we can find the distance between the bottom of the deflected membrane and the top of the oxide layer (Fig. 1), which gives a rough indication of the maximum possible downward ac membrane displacement. From this maximum displacement, we can estimate the

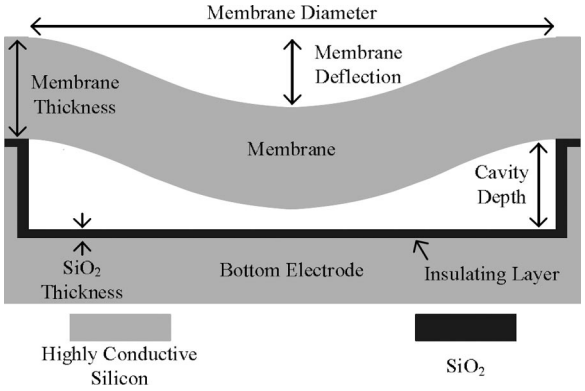

Fig. 1. A simplified diagram of a CMUT cell illustrating its key dimensions. Each 100-mm wafer contains 4 quadrants with 71 parallel-connected CMUT cells. We designed the CMUT cell's dimensions for a collapse voltage of less than 1000 V and an operating frequency close to 50 kHz.

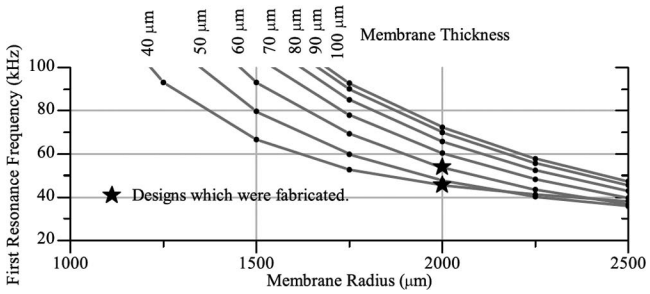

Fig. 2. Finite element model (FEM) simulation results of the fundamental mode resonance frequency (calculated using a prestressed modal analysis) as a function of membrane thickness and radius.

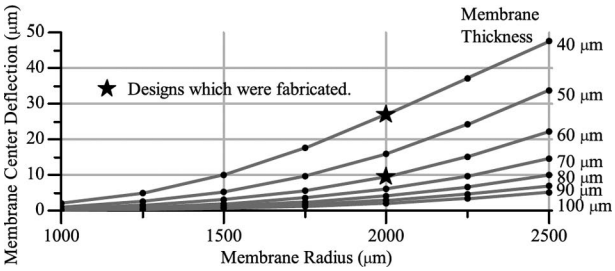

Fig. 3. Finite element model (FEM) simulation results of membrane displacement due to atmospheric pressure as a function of membrane thickness and radius. Because the CMUT cavities are sealed in a low pressure environment (less than 10^{-5} mBar), atmospheric pressure significantly deflects the membranes.

maximum displacement spatially averaged over the entire device using

$$d_{\mathrm{avg,ac}} = (d_{\mathrm{cav}} - d_{\mathrm{atm}} - d_{\mathrm{dc}}) r_{\mathrm{fill}} / r_{\mathrm{pk2avg}}, \qquad (1)$$

which in turn allows us to estimate the maximum output pressure of the device. In (1), $d_{\mathrm{avg,ac}}$ is the maximum spatially averaged membrane displacement, d_{cav} is the cavity depth, d_{atm} is the deflection due to atmospheric pressure, and d_{dc} is the deflection due to dc bias.

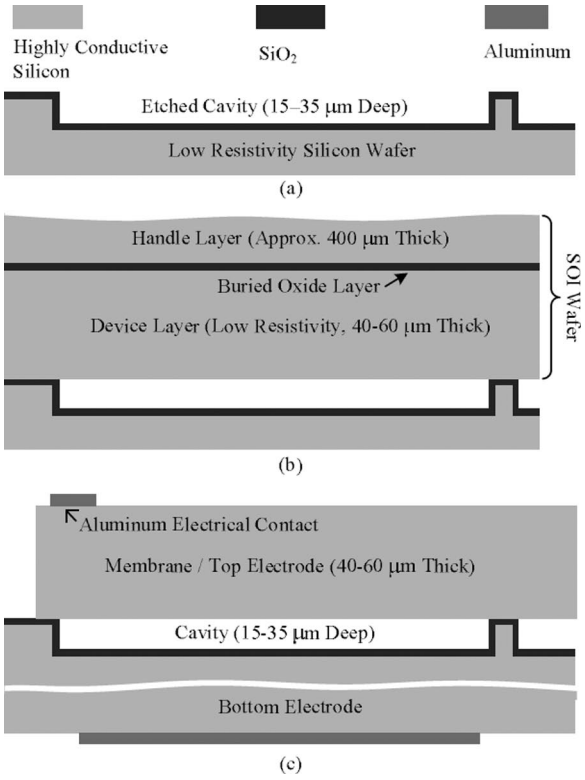

Fig. 4. The device fabrication process: (a) The process starts with a low resistivity silicon wafer. (b) Deep reactive ion etching (DRIE) creates the cavities; thermal oxidation produces a 3.3-μm-thick insulating oxide layer. (c) Wafer bonding permanently bonds a silicon-on-insulator (SOI) wafer to the wafer with the cavities. (d) A combination of wafer grinding, chemical etching, and reactive ion etching removes the handle and buried oxide layers of the SOI wafer, revealing the device's membrane. Evaporated and patterned aluminum electrodes provide electrical contact to the device.

The fill factor, r_{fill}, is the fraction of the device area occupied by membranes; in this case, the layout of the circular membranes has a fill factor of 88%. The value of r_{pk2avg} gives the ratio of peak ac displacement at the membrane center to displacement averaged over the entire membrane—the membrane moves up and down more at the center than at the edge. We estimated r_{pk2avg} with the FEM for small changes in dc bias voltage.

From the average displacement, (2) gives the magnitude of the RMS acoustic pressure averaged over the transducer surface, where Z_{air} is the acoustic impedance of air, and f is frequency.

$$P_{\text{avg}} = 2\pi f d_{\text{avg,ac}} Z_{\text{air}}/\sqrt{2} \tag{2}$$

Because the transducer is much larger than the wavelength of 50 kHz ultrasound in air (6.9 mm), we use the plane wave acoustic impedance of air, which is 413 Rayls. Table II summarizes the pressure calculations.

These calculations give only a rough estimate of maximum achievable acoustic pressure. However, they help guide the device design, and ultimately the predicted values match the measured results with reasonable accuracy.

Generating higher sound pressure levels requires a larger gap and higher ac and dc voltages. The thickness and quality of the insulating oxide determines the maximum voltages the CMUT can withstand before breakdown. The theoretical breakdown voltage of SiO_2 is about 1000 V/μm; we have observed breakdown voltages closer to 400 V/μm for devices fabricated in our facilities. For the CMUTs presented in this paper, we chose an oxide thickness of 3.3 μm, which is thicker than required based on a 400 V/μm breakdown voltage and the simulated collapse voltages. If we assume the density of defects in the oxide is constant, a larger area of oxide has a higher number of defects. Additionally, a larger area of oxide has greater exposure to contamination. Thus, because the CMUTs are much larger than typical CMUTs, we used a thick insulating oxide layer.

III. Fabrication

We used a fabrication process (Fig. 4) based on direct wafer bonding to fabricate the CMUTs. The most challenging aspects of the fabrication were a result of the CMUT's large size. Each 100 mm wafer comprises only 4 devices, and a short or defect in the insulating oxide at any point on a device affects the device as a whole. We adapted several steps of the fabrication process to address the challenge of making large devices with good yield.

The process started with a low resistivity (approximately 0.02 Ω-cm or less) silicon wafer, as shown in Fig. 4(a). Because this wafer is the bottom electrode of the CMUT, the resistivity must be low enough so that the entire wafer can be considered electrically connected. The cavities were defined using optical lithography and then etched with deep reactive ion etching (DRIE) equipment (Multiplex Pro ASE HRM Deep Reactive Ion Etcher, Surface Technology Systems, Newport, UK). We used DRIE because it quickly and reliably creates deep cavities. However, for the devices described here and the DRIE recipe used, there was variation in cavity depth across the wafer. The depth of the etched cavities excluding those at the wafer's edge were within 6% of the mean cavity depth. The cavities at the edge were about 10% to 12% deeper than the mean depth. After the cavities were etched, a 3.3-μm-thick SiO_2 layer was grown at 1100°C in a wet oxidation furnace, as shown in Fig. 4(b).

We then bonded (model SB6 wafer bonder, Karl Süss, Garching, Germany) the oxidized wafer to an SOI wafer, as shown in Fig. 4(c). Bonding was done with a force of 600 N at a temperature of 50°C and a pressure of less than 10^{-5} mbar. Annealing the wafers in a dry oxidation furnace for 3 h at 1050°C resulted in a permanent fusion bond between the wafers.

Next, we removed the handle and buried oxide layers of the SOI wafer. We used wafer grinding to remove all but 100 μm of the handle layer. The remaining handle wafer silicon was etched away with tetramethylammonium hydroxide (TMAH); the buried oxide layer acted as an etch

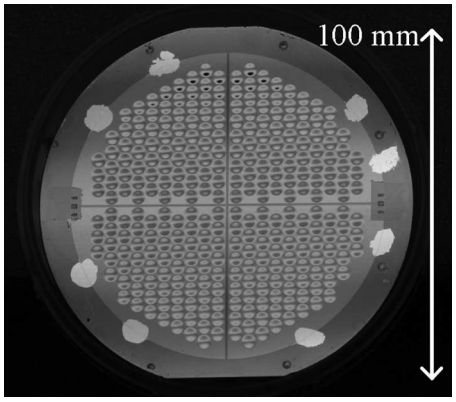

Fig. 5. A photograph of a completed device. The device is divided into 4 quadrants. The bright spots around the wafer edge are the aluminum electrodes. The deflection of the membranes from atmospheric pressure is clearly visible.

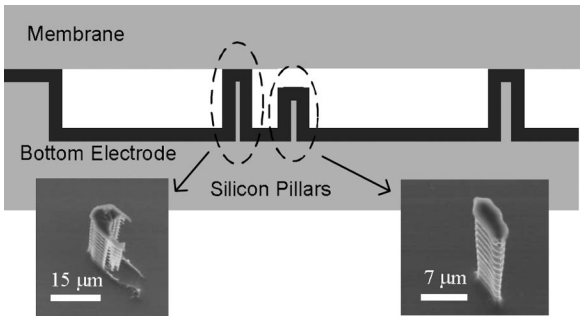

Fig. 6. Illustration and scanning electron micrographs (SEMs) of the silicon pillars. Photoresist or particles in the cavity region before the cavity etch mask the etching and result in tall pillars of silicon. These pillars obstruct the membrane's deflection and can reduce the device's breakdown voltage. We modified the lithography and etch steps of the fabrication process to eliminate the pillars.

stop for the TMAH. Dry oxide etching removed the buried oxide layer, revealing the membranes. In some cases, some of the revealed membranes near the wafer edge were broken, which was probably a result of poor wafer bonding in those regions. We covered the regions with broken membranes with polyimide tape to protect the exposed cavity oxide from subsequent etching. Furthermore, we avoided wet oxide etchant because it can flow into the cavities with broken membranes.

In the final steps, we divided the wafer into quadrants and created aluminum electrodes. We used reactive ion etching to remove the conductive membrane silicon between the wafer quadrants and around the wafer perimeter where it could short with the back side electrodes. We then used reactive ion etching to open up areas of oxide on the wafer back side for the aluminum electrodes, as shown in Fig. 4(d). Evaporated and patterned aluminum on the top and bottom of the wafer formed the electrodes, at which point the device was finished (Fig. 5) and ready for testing.

In developing the fabrication process, our biggest challenge was to etch the cavities without leaving pillars of unetched silicon (Fig. 6). These pillars result from leftover photoresist or particles present in the cavity regions that act as a mask to the DRIE cavity etching; they obstruct the membrane deflection and, if not covered with thick oxide, can short the device or limit its breakdown voltage. The large device area makes it particularly challenging to ensure a device is free of pillars. In our first fabrication run, we counted about 40 points on the wafer where the pillars could be seen obstructing the membrane's deflection.

Most of the pillars can be prevented in the lithography step used to define the cavity areas. For this lithography, we used a second exposure to ensure that no unexposed photoresist was left in the cavity areas. Between exposures, we rotated the mask used for the photolithography 180° (the mask is symmetric) to ensure that defects on the mask do not result in unexposed photoresist. Furthermore, we cleaned the mask before each exposure.

Even with careful particle prevention and attention to the cavity lithography step, silicon pillars appeared after an anisotropic DRIE cavity etch (Fig. 6). To prevent these pillars, we switched to an isotropic DRIE cavity etch. Isotropic etching undercuts defects on the wafer that are small relative to the cavity depth and thus etches away pillars that are tall and narrow.

When we used a second exposure for the cavity lithography combined with isotropic cavity etching, most of the fabricated wafers had no observable pillars. The remaining pillars are covered with a thick layer of oxide and thus do not short the device.

IV. Measurement Results and Discussion

We fabricated and characterized devices with the two designs given in Table I. We first characterized the devices by measuring their electrical input impedance with an impedance analyzer (Agilent 4294A, Agilent Technologies, Palo Alto, CA). The design-A input impedance is shown in Fig. 7 (the design-B device suffered an oxide breakdown, as described in Section IV, before we obtained an accurate input impedance measurement). The design-A input impedance shows a peak at the resonance frequency. In addition, it has small off-resonance peaks, which are partly a result of variations in membrane thickness and cavity depth between CMUT cells. For example, membranes at the wafer's edge have a higher resonance frequency because they experience less spring softening (spring softening is the reduction in resonance frequency as the applied dc bias voltage approaches the collapse voltage [37]). Edge membranes experience less spring softening because they have deeper cavities, and thus the applied DC bias is a smaller fraction of their collapse voltage.

To measure output pressure and beam patterns, we mounted the devices on a rotational stage and measured their output with a calibrated microphone (1/4-in. Free Field Microphone Type 40 BF, G.R.A.S. Sound and Vibration, Vedbaek, Denmark). A function generator (model 33250A, Agilent Technologies, Palo Alto, CA) followed by

TABLE III. SUMMARY OF MEASUREMENTS.

Design	A	B
Atmospheric Deflection (μm)	29.1	10.1
AC excitation (V peak-to-peak)	200	200
DC bias (V)	380	350
Center frequency (kHz)	46	55
Bandwidth (kHz)	2.0	5.4
Pressure at 3 m (dB re 20 μPa RMS)	114	107
Pressure normalized to 0 m (dB re 20 μPa RMS)	135	129

an amplifier (DCA-50R, Krohn-Hite Corporation, Brockton, MA) generated a 200-V peak-to-peak ac excitation voltage. As we increased the applied dc bias voltage, the pressure produced by the CMUTs increased until a saturation point was reached, where further increases in dc bias voltage resulted in only small gains in measured acoustic pressure. We set the dc bias voltage to the start of this saturation point, which occurred at about 350 V, to minimize the risk of electrical breakdown of the oxide insulation layer.

At a distance of 3 m, we used the microphone to measure the acoustic pressures generated by the CMUTs as a function of ac excitation frequency (Fig. 8 and Table III). For these measurements, we excited just 2 of the 4 wafer quadrants in parallel to characterize the wafer halves separately and to decrease the risk of damaging the entire wafer. The measured frequency responses show that the fabricated CMUTs have center frequencies close to the resonance frequencies predicted by finite element modeling (Table II). To estimate the acoustic pressure generated at the face of the CMUTs, we simulated the source sound pressure levels needed to generate the sound pressure levels measured at 3 m (the simulation method based on the KZK equation is described below). At 3 m, the design-A and design-B CMUTs produced 114 dB and 107 dB, respectively. From these levels, our simulations predict average acoustic source levels at the face of the devices of 135 dB and 129 dB, respectively.

At the face of the devices, the design-A and design-B CMUTs produced estimated average acoustic source levels of 135.3 dB and 128.9 dB, respectively. Measurements made with an interferometer of displacement at different positions on the wafer indicate that membranes at the edge have about one-half the displacement of membranes in the center; this variation in displacement results from the variation in cavity depth described in Section III. When we account for this variation in displacement across the wafer, the estimated acoustic source levels at the center of the wafer for the design-A and design-B CMUTs is 138.1 dB and 131.5 dB, respectively.

Both designs produced less sound pressure than the maximum values predicted by the design calculations (Table II). The lower measured sound pressures are likely due to variations in cavity depth and the limited 200 V ac excitation voltage. Because the center frequency of individual cells varies with their position on the wafer, as a result of variation in cavity depths across the wafer, and because each cell has a relatively narrow frequency response, only

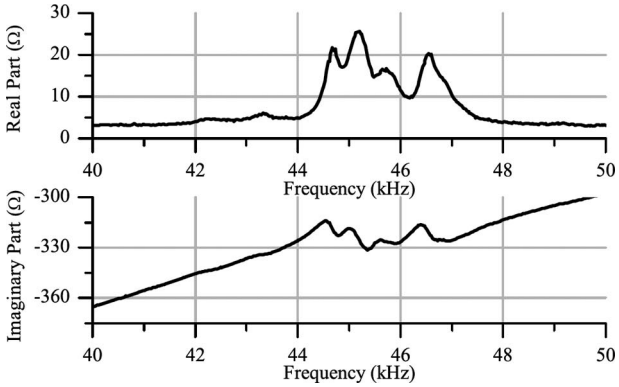

Fig. 7. Measured input impedance (design A) for 2 of the 4 wafer quadrants connected in parallel.

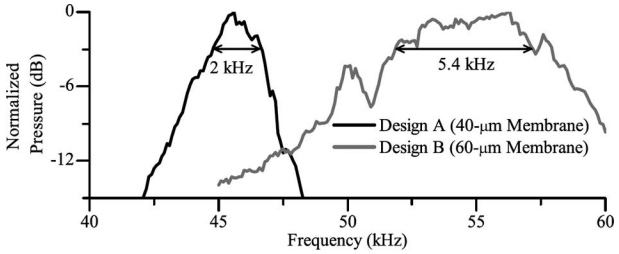

Fig. 8. Frequency responses of the CMUTs determined by measuring the sound pressure level at 3 m as a function of ac excitation frequency.

a fraction of the cells operate at their center frequency for a single-frequency excitation. This effect increases the bandwidth of the device as a whole but results in lower total output sound pressure at any single frequency.

The variation in cavity depth affects the design-B device more than the design-A device. The design-B device has a lower collapse voltage, and thus for the same dc bias voltage, the design-B device is closer to the collapse point, where a cell's center frequency is more sensitive to bias voltage. Furthermore, the membrane of the design-B device is thicker, and thus the cells have a narrower frequency response. As a result, they produce less pressure if operated at a frequency away from their center frequency. Because the cavity depth variation affects the design-B device more, it produced comparatively less pressure than expected and had a wider bandwidth, despite having a thicker membrane.

The cavity depth variation may also contribute to the observed saturation in sound pressure level for increasing dc bias voltage. At the saturation point, some of the cells begin to operate at their peak displacement. Additionally, for increasing dc bias, the variation in center frequency from cell-to-cell increases because the dc voltage is closer to the collapse voltage.

Larger ac-excitation voltages would help generating increased sound pressure levels. A membrane's displacement is proportional to the product of the ac excitation voltage and the dc bias voltage. Thus, if we could increase the ac voltage beyond 200 V peak-to-peak, we could decrease the dc voltage and achieve the same displacement. A de-

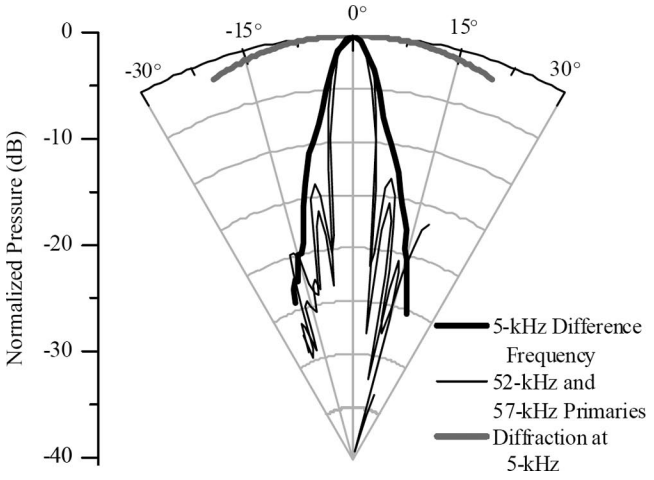

Fig. 9. Primary and difference frequency beam patterns at 3 m. We drove a design-B device with the sum of 52 kHz and 57 kHz 100-V peak-to-peak sinusoidal signals to create a 5 kHz parametric array. On-axis 3 m from the CMUT source, the sound pressure levels of the primary frequencies were 100 dB and 108 dB relative to 20 μPa RMS, respectively. The sound pressure level of the 5 kHz difference frequency was 58 dB. The diffraction curve shows the 5 kHz sound beam profile had that frequency of sound been directly radiated by the source. Comparison of the diffraction curve with the measured sound beam profile clearly illustrates that the parametric array results in a much narrower beam of sound than conventional sound transmission.

creased dc voltage would make the device less sensitive to cavity depth variations. Additionally, a smaller dc voltage would result in less static deflection, leaving more room for displacement.

We used a design-B CMUT to transmit 5 kHz sound with a parametric array. The sum of two 100 V ac excitation signals 5 kHz apart in frequency drove the 4 quadrants of the CMUT. The resulting primary frequency and difference frequency beam patterns (Fig. 9) demonstrate transmission of a narrow beam of sound. We could clearly hear the 5 kHz sound along the CMUT's axis; at 3 m, the level of the 5 kHz sound was 58 dB. For comparison, the sound level of normal conversation is about 60 dB.

For these beam pattern measurements, we excited the entire CMUT with the sum of the primary signals. Ideally, the primaries would be transmitted from separate interleaved parts of the transducer to prevent nonlinearities in the transducer from directly radiating sound at the difference frequency. A comparison between driving the CMUT with the sum of the primary frequency signals and driving separate wafer quadrants with separate primary signals showed that driving the CMUT with the sum resulted in similar sound pressure levels at the difference frequency and just a slightly wider sound beam, indicating transducer nonlinearities were not a significant source of difference frequency sound.

Nonlinearities at the receiver can also result in spurious difference-frequency sound generation. Bennett and Blackstock noted 2 sources of difference-frequency sound at the receiver; both are associated with the primary waves' interaction with the microphone [28]. The first source is due to nonlinearity in the microphone and its electronics; the second source is due to acoustic radiation pressure—Westervelt referred to the latter as pseudosound [39]. Because both sources are proportional to the product of the 2 primary wave amplitudes at the location of the microphone, their spatial dependencies are indistinguishable. We therefore refer to spurious difference-frequency generation at the receiver generically as detector nonlinearity, irrespective of whether it is due to pseudosound or nonlinearity in the receiver system.

Detector nonlinearity results in a directivity function for the difference frequency that is proportional to the product of the directivity functions of the 2 primary frequencies. Thus, the resulting difference frequency beamwidth is narrower than that for either primary frequency. The resulting beamwidth is also narrower than the beamwidth of the difference frequency generated by the parametric array. Because the effect of the parametric array relative to detector nonlinearity increases with distance from the source, we expect the difference frequency beamwidth to increase with distance. And, indeed, we observed that the beamwidth at the difference frequency increased from about 7° at 1 m to 9° at 3 m as sound resulting from detector nonlinearity gave way to sound from the parametric array.

To remove the contribution of microphone nonlinearity to detector nonlinearity, an acoustic low-pass filter can be placed in front of the microphone. This filter passes the difference frequencies but attenuates the high-intensity primary waves that result in spurious difference frequency generation due to the microphone's nonlinearity. In [28], Bennett and Blackstock use cellophane plastic as the acoustic filter. In [40], Havelock and Bramme use layers of felt. In [41], Toda discusses the design of an acoustic filter made from layers of polymer. He uses the filter to show the relative contributions of microphone nonlinearity, radiation pressure, and the parametric array to measured sound pressure levels at the difference frequency. For the study presented in this paper, we used a thin sheet of Saran film for the acoustic filter.

We made measurements of the sound pressure levels at the difference frequency, both with and without the acoustic filter, as a function of distance along the beam axis and compared the results with simulations (Fig. 10). For these measurements, we generated the primary waves with separate quadrants of the source transducer. Numbered in the clockwise direction, quadrants 1 and 3 radiated one primary frequency, and quadrants 2 and 4 radiated the other primary frequency such that the source geometry for each primary wave resembled a bow tie. This configuration was used to avoid any possibility of the source producing difference frequency directly due to its inherent nonlinearity. Additionally, it interleaved the sources of the 2 primary frequencies to the greatest extent possible with the given source design.

The curves shown in Fig. 10 are simulations obtained from numerical solutions of the KZK equation that account for nonlinearity, diffraction, thermoviscous absorption, and atmospheric absorption due to molecular relax-

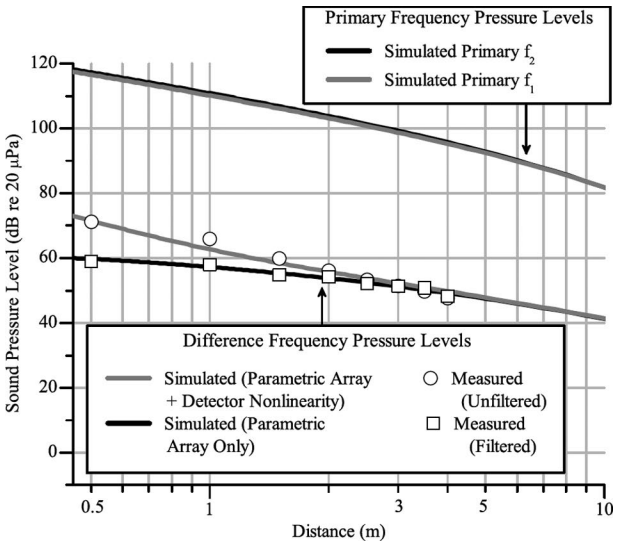

Fig. 10. Sound pressure levels of the primaries (f_1 = 48.5 kHz, f_2 = 53.5 kHz) and 5 kHz difference frequency as a function of distance from the CMUT. Close to the CMUT, where the sound pressure levels of the primary waves are high, detector nonlinearity is the dominant source of measured sound level at the difference frequency. We placed an acoustic low-pass filter in front of the microphone to attenuate the sound at the primary frequencies incident on the microphone, and thus also the effect of detector nonlinearity. The remaining sound comes from the parametric array.

ation [42]. Although the specific numerical algorithm we used simulates axisymmetric sound fields, it proved to be sufficiently accurate for difference frequency calculations despite the asymmetry of the source geometry. We thus modeled the source as a circular disk of diameter 5.3 cm to match the surface area of each bow tie, which is to say that we divided the diameter of the active area of the full circular CMUT, 7.5 cm, by $\sqrt{2}$. We then chose the source levels that produced the best fit with the measurements at the difference frequency, and these were found to be 121 dB at each of the primary frequencies used for these measurements, 48.5 kHz and 53.5 kHz.

For the stated source conditions, we simulated the sound pressure level at the difference frequency due to the parametric array effect alone, which we denote by p_{pa}, and the sound pressure level due to the combination of the parametric array and detector nonlinearity, which we denote by p_{per}, where $p_{\mathrm{per}} = p_{\mathrm{pa}} + p_{\mathrm{dn}}$. We assume a quadratic component dominates the detector nonlinearity, p_{dn}. Therefore, we model the detector nonlinearity using $p_{\mathrm{dn}} = Kp_1p_2$, where p_1 and p_2 are the peak pressure amplitudes of the primary waves at the microphone location, and K is a constant determined by best fit with the measurements. From the measurements shown in Fig. 10, we determined that $K = 2 \times 10^{-4}$ Pa^{-1}. For this value of K, the simulated difference frequency sound levels match the measured levels very well with distance (Fig. 10). We thus observe how detector nonlinearity dominates the measurements close to the source. However, beyond about 3 m its effect is negligible, and only the contribution from the parametric array is measured at the difference frequency.

Having found a value for K that agrees with the measured pressure levels, we can investigate the source of detector nonlinearity. Consider first the contribution due to radiation pressure (pseudosound). The radiation pressure on a surface (e.g., the face of a microphone) due to reflection of a sound beam is taken to be $p_{\mathrm{rad}} = 2\langle E\rangle$ [43], where $\langle E\rangle$ is the time-averaged energy density in the incident beam. When evaluated for the radiation pressure at the difference frequency, the relationship may be rewritten as $p_{\mathrm{rad}} = K_{\mathrm{rad}}p_1p_2$, where $K_{\mathrm{rad}} = 1.4 \times 10^{-5}$ Pa^{-1} for air at room temperature. Because $K_{\mathrm{rad}} = 0.07K$, the contribution due to radiation pressure is too low to account for the detector nonlinearity. Now observe from Fig. 10 that the levels of the difference frequency due to detector nonlinearity are about 45 to 50 dB below the peak level in the primary beam. The corresponding harmonic distortion is thus between 0.3% and 0.6% in terms of amplitude ratio. Because our microphone specifications state only that the total harmonic distortion is less than 1%, it is most likely that the source of our detector nonlinearity was the microphone assembly, which includes the capacitive transducer and preamplifier. In [41], Toda also shows that without an acoustic filter, microphone nonlinearity dominates the effect of radiation pressure.

Because the relative contributions of detector nonlinearity and the parametric array vary with distance from the source, the frequency response of the directional sound also varies with distance. This frequency dependence means that the perceived sound pressure level at the difference frequency for fixed primary source levels varies with the difference frequency. As discussed in [41], the detector nonlinearity contribution of the sound pressure level (characterized by the constant K) has very little frequency dependence because radiation pressure is independent of frequency and because we expect microphone nonlinearity to vary weakly with frequency. The contribution to the sound pressure level generated by the parametric array, which dominates for distances far from the source, varies with frequency in proportion to f_{diff}^n, where n depends primarily on the ratio of diffraction length (the area of the transmitter divided by the wavelength at the primary frequencies) to absorption length (the inverse of the nominal absorption coefficient at the primary frequencies). When the ratio is large, the Westervelt solution [26], [27], for which $n = 2$, is a good approximation of the frequency dependence. When the ratio is small, the solution obtained by Berktay and Leahy [44], for which $n = 1$, is a good approximation. In practice, the result lies somewhere in between.

Numerical solutions of the KZK equation for the conditions of our experiments indicate $n \simeq 1.5$, which predicts that the sound pressure level at the difference frequency will increase by 9 dB per octave. The significance of n for audio applications is that it is also the order of the time derivative that, when applied to the square of the envelope modulating the amplitude of the carrier wave, yields the demodulated acoustic waveform along the axis of the

parametric array. It therefore suggests the form of predistortion required for the transmission of speech.

To examine the frequency dependence experimentally, we measured unfiltered sound pressure levels at difference frequencies of 1 kHz, 3 kHz, and 5 kHz at distances from 0.5 m to 2.5 m. Because the sound pressure levels at the primary frequencies varied slightly between experiments, we normalized the measured sound pressures at the difference frequency by the product of sound pressures at the primary frequencies. At 0.5 m, the normalized sound levels at the 3 difference frequencies were within 1 dB of each other. We expected a lack of frequency dependence at this distance, where detector nonlinearity dominates the effect of the parametric array. At 2.5 m, where the relative effect of the parametric array is more significant, the sound level at 5 kHz was 3.5 dB higher than at 3 kHz and 7 dB higher than at 1 kHz. This dependence on frequency is weaker than $f_{\text{diff}}^{1.5}$ because at 2.5 m detector nonlinearity still contributes to the measured difference frequency signal.

We made most of the measurements for this study using a 5 kHz difference frequency because it results in high sound pressure levels that are easy to measure over a range of distances and detector angles. However, transmission of intelligible speech would require a bandwidth that extends from about 1 kHz to 4.5 kHz [45]. At 3 m, we produced 5 kHz sound pressure levels up to 58 dB. Transmission of speech at similar sound pressure levels and across similar distances requires higher source pressure levels at the primary frequencies, particularly for frequencies at the low end of the frequency spectrum of speech. Because the difference-frequency pressure increases with the surface area of the source (it is proportional to source area in Westervelt's model [27]), tiling together rectangular-shaped CMUTs to create a larger source would be one way to achieve higher levels at the difference frequency. Based on our measurements made at 5 kHz, we expect doubling the source diameter and generating sound pressure levels equal to the maximum levels measured for the design-A device would be sufficient for transmitting speech across several meters. Alternatively, CMUTs with a thicker insulating layer and deeper cavities could be designed to produce higher source levels with larger excitation voltages.

Redesigned CMUTs may also use a thicker oxide layer to extend their operating time until breakdown. For characterization of the CMUTs, we operated them for hours to tens of hours with large excitation voltages. However, for most of the wafers, the insulating oxide in at least one of the wafer quadrants eventually broke down. The oxide typically broke down after prolonged operation with a 350 V dc bias voltage and a 200 V peak-to-peak ac excitation voltage. A total voltage of 550 V across a 3.3-μm-thick insulating oxide corresponds to an electric field of 167 V/μm. This electric field is well below the 400 V/μm breakdown electric field we expected based on past CMUT designs. The large area covered by the oxide and the silicon pillars discussed in Section III are possible reasons for the reduced breakdown voltage. Additionally, exposed oxide between the wafer quadrants and at the wafer edge may become contaminated over time. A passivating layer of silicon nitride would prevent this contamination.

V. Conclusion

The results presented in this paper demonstrate that, with wafer-bonding fabrication methods, we can make low-frequency CMUTs to transmit sound using a parametric array. The large area of the CMUTs presented the biggest fabrication challenge. We learned that each fabrication step should be adapted to prevent defects. Furthermore, the device should be robust enough to tolerate the fabrication defects that cannot be prevented.

The CMUTs produced high-intensity 50 kHz ultrasound sufficient to transmit a narrow beam of clearly audible 5 kHz sound with a parametric array over several meters. To transmit wideband audio, such as speech, over similar distances, several CMUT devices could be combined to create a large-area source. Alternatively, the CMUTs could be redesigned to generate higher pressures with larger excitation voltages. Currently, we are exploring methods of modulating the primaries for wideband sound transmission [30] and continuing to develop CMUT technology with the goal of making a compact source of highly directional sound.

References

[1] T. Yano, M. Tone, and A. Fukumoto, "Range finding and surface characterization using high-frequency air transducers," *IEEE Trans. Ultrason. Ferroelectr. Freq. Control*, vol. 34, no. 2, pp. 232–236, 1987.

[2] B. T. Khuri-Yakub, J. H. Kim, C.-H. Chou, P. Parent, and G. S. Kino, "A new design for air transducers," in *Proc. 1988 IEEE Ultrasonics Symp.*, vol. 1, pp. 503–506.

[3] M. Toda, "New type of matching layer for air-coupled ultrasonic transducers," *IEEE Trans. Ultrason. Ferroelectr. Freq. Control*, vol. 49, no. 7, pp. 972–979, 2002.

[4] M. I. Haller and B. T. Khuri-Yakub, "Micromachined 1–3 composites for ultrasonic air transducers," *Rev. Sci. Instrum.*, vol. 65, no. 6, pp. 2095–2098, 1994.

[5] J. Kritz, "A high-efficiency transducer for transmission to air," *IRE Trans. Ultrason. Eng.*, vol. 8, no. 1, pp. 14–18, 1961.

[6] C. Germano, "Flexure mode piezoelectric transducers," *IEEE Trans. Audio Electroacoust.*, vol. 19, no. 1, pp. 6–12, 1971.

[7] R. Takayama, A. Tokushima, N. Ueshiba, and Y. Ise, "Ultrasonic transducer of piezoelectric ceramic for pulse driving: Ultrasonic imaging," *Jpn. J. Appl. Phys., Suppl.*, vol. 21, no. 3, pp. 167–169, 1982.

[8] H. Okada, M. Kurosawa, S. Ueha, and M. Masuda, "New airborne ultrasonic transducer with high output sound pressure level," *Jpn. J. Appl. Phys.*, vol. 33, no. 5, pp. 3040–3044, 1994.

[9] J. J. Bernstein, S. L. Finberg, K. Houston, L. C. Niles, H. D. Chen, L. E. Cross, K. K. Li, and K. Udayakumar, "Micromachined high frequency ferroelectric sonar transducers," *IEEE Trans. Ultrason. Ferroelectr. Freq. Control*, vol. 44, no. 5, pp. 960–969, 1997.

[10] G. Percin and B. T. Khuri-Yakub, "Piezoelectrically actuated flextensional micromachined ultrasound transducers. I. theory," *IEEE Trans. Ultrason. Ferroelectr. Freq. Control*, vol. 49, no. 5, pp. 573–584, 2002.

[11] G. Percin and B. T. Khuri-Yakub, "Piezoelectrically actuated flextensional micromachined ultrasound transducers. II. Fabrication and experiments," *IEEE Trans. Ultrason. Ferroelectr. Freq. Control*, vol. 49, no. 5, pp. 585–595, 2002.

[12] M. Toda, "Phase-matched air ultrasonic transducers using corrugated pvdf film with half wavelength depth," *IEEE Trans. Ultrason. Ferroelectr. Freq. Control*, vol. 48, no. 6, pp. 1568–1574, 2001.
[13] M. Toda, "Cylindrical PVDF film transmitters and receivers for air ultrasound," *IEEE Trans. Ultrason. Ferroelectr. Freq. Control*, vol. 49, no. 5, pp. 626–634, 2002.
[14] E. Fukada, "History and recent progress in piezoelectric polymers," *IEEE Trans. Ultrason. Ferroelectr. Freq. Control*, vol. 47, no. 6, pp. 1277–1290, 2000.
[15] R. G. Swartz and J. D. Plummer, "On the generation of high-frequency acoustic energy with polyvinylidene fluoride," *IEEE Trans. Sonics Ultrason.,* vol. 27, no. 6, pp. 295–302, 1980.
[16] A. Gachagan, G. Hayward, S. P. Kelly, and W. Galbraith, "Characterization of air-coupled transducers," *IEEE Trans. Ultrason. Ferroelectr. Freq. Control*, vol. 43, no. 4, pp. 678–689, 1996.
[17] M. Rafiq and C. Wykes, "The performance of capacitive ultrasonic transducers using v-grooved backplates," *Meas. Sci. Technol.*, vol. 2, no. 2, p. 168, 1991.
[18] H. Carr and C. Wykes, "Diagnostic measurements in capacitive transducers," *Ultrasonics*, vol. 31, no. 1, pp. 13–20, 1993.
[19] K. Suzuki, K. Higuchi, and H. Tanigawa, "A silicon electrostatic ultrasonic transducer," *IEEE Trans. Ultrason. Ferroelectr. Freq. Control*, vol. 36, no. 6, pp. 620–627, 1989.
[20] D. W. Schindel, D. A. Hutchins, L. Zou, and M. Sayer, "The design and characterization of micromachined air-coupled capacitance transducers," *IEEE Trans. Ultrason. Ferroelectr. Freq. Control*, vol. 42, no. 1, pp. 42–50, 1995.
[21] M. J. Anderson, J. A. Hill, C. M. Fortunko, N. S. Dogan, and R. D. Moore, "Broadband electrostatic transducers: Modeling and experiments," *J. Acoust. Soc. Am.*, vol. 97, no. 1, pp. 262–272, 1995.
[22] A. Schröder, S. Harasek, M. Kupnik, M. Wiesinger, E. Gornik, E. Benes, and M. Gröschi, "A capacitance ultrasonic transducer for high-temperature applications," *IEEE Trans. Ultrason., Ferroelect., Freq. Contr.*, vol. 51, no. 7, pp. 896–907, 2004.
[23] M. I. Haller and B. T. Khuri-Yakub, "A surface micromachined electrostatic ultrasonic air transducer," *IEEE Trans. Ultrason. Ferroelectr. Freq. Control*, vol. 43, no. 1, pp. 1–6, 1996.
[24] R. A. Noble, A. D. R. Jones, T. J. Robertson, D. A. Hutchins, and D. R. Billson, "Novel, wide bandwidth, micromachined ultrasonic transducers," *IEEE Trans. Ultrason. Ferroelectr. Freq. Control*, vol. 48, no. 6, pp. 1495–1507, 2001.
[25] A. S. Ergun, Y. Huang, X. Zhuang, O. Oralkan, G. G. Yaraholu, and B. T. Khuri-Yakub, "Capacitive micromachined ultrasonic transducers: Fabrication technology," *IEEE Trans. Ultrason. Ferroelectr. Freq. Control*, vol. 52, no. 12, pp. 2242–2258, 2005.
[26] P. J. Westervelt, "Parametric end-fire array," *J. Acoust. Soc. Am.,* vol. 32(A), no. 7, pp. 934–935, 1960.
[27] P. J. Westervelt, "Parametric acoustic array," *J. Acoust. Soc. Am.*, vol. 35, no. 4, pp. 535–537, 1963.
[28] M. B. Bennett and D. T. Blackstock, "Parametric array in air," *J. Acoust. Soc. Am.*, vol. 57, no. 3, pp. 562–568, 1975.
[29] M. Yoneyama, J.-I. Fujimoto, Y. Kawamo, and S. Sasabe, "The audio spotlight: An application of nonlinear interaction of sound waves to a new type of loudspeaker design," *J. Acoust. Soc. Am.*, vol. 73, no. 5, pp. 1532–1536, 1983.
[30] T. D. Kite, J. T. Post, and M. F. Hamilton, "Parametric array in air: Distortion reduction by preprocessing," in *Proc. 16th Int. Congr. Acoustics*, 1998, New York, pp. 1091–1092.
[31] F. J. Pompei, "The use of airborne ultrasonics for generating audible sound beams," *J. Audio Eng. Soc.*, vol. 47, no. 9, pp. 726–731 1999.
[32] F. J. Pompei, "Sound from ultrasound: The parametric array as an audible sound source," Ph.D. dissertation, Massachusetts Institute of Technology, Cambridge, MA, 2002.
[33] W. Kim and V. W. Sparrow, "Audio application of the parametric array–implementation through a numerical model," presented at the 113th Audio Engineering Society Convention, Los Angeles, 2002.
[34] M. F. Hamilton and D. T. Blackstock, *Nonlinear Acoustics*. New York: Academic Press, 1998.
[35] H. E. Bass, L. C. Sutherland, A. J. Zuckerwar, D. T. Blackstock, and D. M. Hester, "Atmospheric absorption of sound: Further developments," *J. Acoust. Soc. Am.*, vol. 97, no. 1, pp. 680–683, 1995.
[36] A. C. Ugural, *Stresses in Plates and Shells*, 2nd ed. Boston: McGraw Hill, 1999.
[37] S. D. Senturia, *Microsystem Design*. New York: Kluwer Academic Publishers, 2001.
[38] *ANSYS 11.0 SP1 Manual*, Ansys Inc., Canonsburg, PA, 2007.
[39] P. J. Westervelt, "Scattering sound by sound," *J. Acoust. Soc. Am.*, vol. 29, no. 2, pp. 199–203, 1957.
[40] D. I. Havelock and A. J. Brammer, "Directional loudspeakers using sound beams," *J. Audio Eng. Soc.*, vol. 48, no. 10, pp. 908–916, 2000.
[41] M. Toda, "New type of acoustic filter using periodic polymer layers for measuring audio signal components excited by amplitude-modulated high-intensity ultrasonic waves," *J. Audio Eng. Soc.*, vol. 53, no. 10, pp. 930–941, 2005.
[42] Y.-S. Lee and M. F. Hamilton, "Time-domain modeling of pulsed finite amplitude sound beams," *J. Acoust. Soc. Am.*, vol. 97, no. 2, pp. 906–907, 1995.
[43] T. G. Wang and C. P. Lee, "Radiation pressure and acoustic levitation," in *Nonlinear Acoustics*, M. F. Hamilton and D. T. Blackstock, Eds. San Diego, CA: Academic Press, 1998, pp. 177–205.
[44] H. O. Berktay and D. J. Leahy, "Farfield performance of parametric transmitters," *J. Acoust. Soc. Am.*, vol. 55, no. 3, pp. 539–546, 1974.
[45] C. V. Pavlovic, "Derivation of primary parameters and procedures for use in speech intelligibility predictions," *J. Acoust. Soc. Am.*, vol. 82, no. 2, pp. 413–422, 1987.

Ira O. Wygant (S'98) received his B.S. degree in electrical engineering with a cross-college major in computer science from the University of Wyoming, Laramie, WY, in 1999. He received his M.S. degree in electrical engineering from Stanford University, Stanford, CA, in 2002. He is currently pursuing a Ph.D. degree in electrical engineering at Stanford University.

He has held internships in the mixed-signal and monolithic sensors group at Oak Ridge National Laboratory, Oak Ridge, TN, in a wireless RF IC design group at Lucent Technologies, Reading, PA, and in the mixed-signal electronics group at Agilent Laboratories, Palo Alto, CA.

His research interests include IC and system design for ultrasound imaging systems based on capacitive micromachined ultrasonic transducers (CMUTs). He was the recipient of a National Science Foundation Graduate Research Fellowship.

Mario Kupnik is currently a research associate in electrical engineering at Edward L. Ginzton Laboratory at Stanford University. He received his Ph.D. degree from the University of Leoben, Austria, in 2004, and the Dipl.Ing. degree from Graz University of Technology in 2000. From summer 1999 to October 2000, he worked as an analog design engineer for Infineon Technologies AG, Graz, on the design of ferroelectric memories and contactless smart card (RFID) systems. His present research interests include the design, modeling, fabrication, and application of micromachined sensors and actuators, with a main focus on capacitive micromachined ultrasonic transducers mainly for air-coupled applications, including high gas temperatures. Examples are transit-time gas flowmeters for hot and pulsating gases, ultrasonic nondestructive evaluation using non-contact ultrasound, nonlinear acoustics, and biochemical gas-sensing applications (electronic nose). Dr. Kupnik has more than 5 years' teaching experience in the field of electrical engineering, and he is a member of the IEEE.

Jeffry C. Windsor was born in Oak Ridge, LA. He received his B.S. degree in physics from Louisiana State University, Baton Rouge, LA, in 1990. In 1992 and 1999, respectively, he received his M.S. and Ph.D. degrees in mechanical engineering at North Carolina State University, Raleigh, NC.

From 1998 to 2001, he worked as an engineer at Ericsson, Inc. in Research Triangle Park, NC, first on the Satellite Phone Development team, then with the Product Reliability and Design Analysis group. Prior to joining Applied Research

Laboratories (ARL:UT) at the University of Texas in Austin, TX, he worked as a project manager and lead programmer for LabVIEW development with Momentum Technical Consulting, Inc. In 2002 he joined ARL:UT as an engineering scientist where he has worked in active sonar analysis and acoustic research, design, and development. He is currently focused on Bayesian tracking.

Dr. Windsor holds one U.S. patent as principal inventor.

Wayne M. Wright holds an appointment as part-time research fellow at the Applied Research Laboratories, University of Texas at Austin. He received the B.A. degree in physics from Bowdoin College in 1956, followed by M.A (1957) and Ph.D. (1961) degrees in applied physics from Harvard University. Now Professor of Physics Emeritus at Kalamazoo College, Kalamazoo, MI, he retired in 1999 after a teaching career that included service as department chair for 20 years. His personal research has generally been in the field of acoustics, with emphasis on experimentation involving high-amplitude sounds. This often has made use of locally constructed ultrasonic transducers that faithfully reproduce signals of large amplitude at frequencies up to almost 1 MHz. Sparks have served as sound sources for many experiments he has performed both at Kalamazoo College and at the University of Texas at Austin. He also has engaged in research in the area of optoacoustics, with faculty at the University of Michigan; in atmospheric acoustics, with NOAA researchers in Boulder, CO; in underwater sound, at the Naval Postgraduate School in Monterey, CA; and in sound absorption in salt solutions such as the ocean, at the University of California in San Diego. Dr. Wright is a Fellow of the Acoustical Society of America, has served as chair of the ASA committees on education, physical acoustics, and prizes and special fellowships, and currently is an elected member of the ASA Executive Council.

Mark Wochner graduated from Vassar College with a B.A. degree in physics in 2001. He received a Ph.D. degree in acoustics from Pennsylvania State University in 2006 and is currently a postdoctoral fellow at the University of Texas at Austin. He is a member of the Acoustical Society of America.

Goksen Goksenin Yaralioglu (S'92–M'99) was born in Akhisar, Turkey on May 13, 1970. He received his B.S., M.S., and Ph.D. degrees from Bilkent University, Ankara, Turkey, in 1992, 1994, and 1999, respectively, all in electrical engineering. He is now working as an engineering research associate in E. L. Ginzton Laboratory, Stanford University, Stanford, CA. His current research interests include design, modeling and applications of micromachined ultrasonic transducers, and atomic force microscopy at ultrasonic frequencies.

Mark F. Hamilton is the Harry L. Kent, Jr. Professor in Mechanical Engineering at the University of Texas at Austin, and he is a research professor at the Applied Research Laboratories, University of Texas at Austin. He received his B.S. degree in electrical engineering from Columbia University in 1978, and his M.S. and Ph.D. degrees in Acoustics from Pennsylvania State University in 1981 and 1983, respectively. He conducts research in physical acoustics, mainly nonlinear acoustics, with a recent emphasis on biomedical acoustics. He has published more than 60 refereed journal articles and 40 conference papers, and he is co-editor of the graduate textbook and research monograph entitled *Nonlinear Acoustics*. He is a recipient of the R. Bruce Lindsay Award of the Acoustical Society of America, the National Science Foundation Presidential Young Investigator Award, the David and Lucile Packard Foundation Fellowship for Science and Engineering, and the ASME Pi Tau Sigma Gold Medal. He began serving a one-year term as president of the ASA in July 2008.

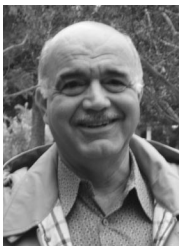

Butrus T. (Pierre) Khuri-Yakub is a professor of electrical engineering at Stanford University. He received the B.S. degree in 1970 from the American University of Beirut, the M.S. degree in 1972 from Dartmouth College, and the Ph.D. degree in 1975 from Stanford University, all in electrical engineering. He was a research associate (1965–1978) then senior research associate (1978–1982) at the E. L. Ginzton Laboratory of Stanford University and was promoted to the rank of professor of electrical engineering in 1982. His current research interests include medical ultrasound imaging and therapy, micromachined ultrasonic transducers, smart bio-fluidic channels, microphones, ultrasonic fluid ejectors, and ultrasonic nondestructive evaluation, imaging and microscopy. He has authored more than 400 publications and has been principal inventor or co-inventor of 76 U.S, and internationally issued patents. He was awarded the Medal of the City of Bordeaux in 1983 for his contributions to Nondestructive Evaluation, the Distinguished Advisor Award of the School of Engineering at Stanford University in 1987, the Distinguished Lecturer Award of the IEEE UFFC society in 1999, a Stanford University Outstanding Inventor Award in 2004, and a Distinguished Alumnus Award of the School of Engineering of the American University of Beirut in 2005.